行政院國家科學委員會專題研究計畫 成果報告

利用高壓合成新穎氫化物材料及其特性分析(台波國合計畫)(2/2)
研究成果報告(完整版)

計 畫 類 別 ：個別型
計 畫 編 號 ：NSC 95-2113-M-002-003-
執 行 期 間 ：95 年 02 月 01 日至 96 年 07 月 31 日
執 行 單 位 ：國立臺灣大學化學系暨研究所

計 畫 主 持 人：劉如熹
共 同 主 持 人：楊弘敦
計畫參與人員：博士班研究生-兼任助理：郭慧通
博士後研究：Nitin C. Bagkar

報 告 附 件 ：國外研究心得報告

處 理 方 式 ：本計畫可公開查詢

中 華 民 國 96 年 09 月 12 日

行政院國家科學委員會補助專題研究計畫 ■ 成 果 報 告
□期中進度報告

（計畫名稱）

利用高壓合成新穎氫化物材料及其特性分析

（台波國合計畫)(2/2)

計畫類別：□ 個別型計畫　　■ 整合型計畫
計畫編號：NSC 95－2113－M－002－003
執行期間： 95 年　2 月　1 日 至　96 年　7 月　31 日

計畫主持人：劉如熹
共同主持人：楊弘敦
計畫參與人員：Nitin C. Bagkar、郭慧通

成果報告類型(依經費核定清單規定繳交)：□精簡報告　■完整報告

本成果報告包括以下應繳交之附件：
■赴國外出差或研習心得報告一份
□赴大陸地區出差或研習心得報告一份
□出席國際學術會議心得報告及發表之論文各一份
□國際合作研究計畫國外研究報告書一份

處理方式：除產學合作研究計畫、提升產業技術及人才培育研究計畫、列管計畫及下列情形者外，得立即公開查詢
□涉及專利或其他智慧財產權，□一年□二年後可公開查詢

執行單位：國立台灣大學化學系

中　華　民　國　96　年　9　月　12　日

目錄

簡介 (Introduction)

Hydrogenation of alloys attracted much interest in recent years due to their importance in both fundamental and application oriented research (1-5). Many researchers focused on the synthesis and characterization of alloys which can accommodate hydrogen under moderate or high pressure conditions in their crystal interstitial sites to act as an effective storage container for hydrogen gas. According to the quantity and applied pressure of the hydrogen loading, crystal lattice can expand considerably. Especially RM_2 (R - rare earth and M - transition metal) Laves phases are very interesting class of materials as they show significant volume expansion, structural changes and varied magnetic properties upon hydrogenation. For these reasons they were studied by many researchers worldwide starting from 1970s (6-10). Magnetic properties are very much variant in these alloys and hydrides with different hydrogen concentration can be formed. For example in YMn_2 Laves phase the magnetic property of the compound is very much dependent on the Mn-Mn distance. The alloy is an itinerant electron antiferromagnet with Mn moment of 2.7 μB (11). When it is hydrogenated on steps, hydrogen atoms will occupy the interstitial sites of crystal lattice and change the crystal structure as well as lattice dimensions (12, 13). Depending on the concentration of hydrogen atoms in the alloy it will expand cell parameters and changes the Mn-Mn distance to considerable extent which ultimately results in significant changes in the magnetic properties due to the critical nature of Mn-Mn interatomic distance (13).

Hydrogen induced structural and magnetic transformations in hexagonal $ErMn_2$ have been reported by Figiel *et al* (14). In $ErMn_2$ they could not observe any magneto-volume effect because magnetic ordering is related to coupling between magnetic moments of Er, and no magnetic moment of manganese exists due to the smaller distance of Mn-Mn than the critical value. Upon H absorption the increase of the Mn-Mn distances causes the appearance of Mn moments which are coupled antiferromagnetically (14). The structural and magnetic properties of $ErMn_2D_{4.2}$ (D = deuteride) and $ErMn_2D_{4.6}$ were studied by neutron diffraction by Makarova

et al. (15). The magnetic structures of the $ErMn_2$ deuterides are very sensitive to the difference of H content: in $ErMn_2D_{4.2}$ there are only short range order magnetic correlations whereas in $ErMn_2D_{4.6}$ sharp magnetic peaks related to an antiferromagnetic structure are observed. This large difference of magnetic structures has been related to the influence of the D atoms on the Mn sublattice and to the large influence of the local hydrogen environment on the first neighbour Mn-Mn interactions. Structural and magnetic properties of $ErFe_2$ hydrides were studied by several researchers (16-19). Five different phases: α (x = 0 to 1), β (x = 1.25 to 2.0), γ (x = 2.25 to 2.75), δ (x = 3.2 to 3.65) and ε (x = 4) were reported for $ErFe_2H_x$ hydride system. The ε phase shows a small rhombohedral distortion while other four phases retain their parent cubic structure (20). Shashikala *et al.* (21) indexed $ErFeH_4$ on the basis of cubic structure with a = 7.92Å. But above x = 4 they could observe the biphasic hydride and stabilized this phase in pure orthorhombic form when x reaches 5 which was the first hydride in this system with orthorhombic structure. The crystal and magnetic structure of $ErFe_2D_5$ were solved by neutron diffraction by Paul-Boncour *et al*. (22) showing a preferential D occupation in some interstitial A_2B_2 and AB_3 sites and an Er order in a canted magnetic structure below 5 K.

The studies related to hydrogen influence on the properties of alloys between $ErFe_2$ and $ErMn_2$ were so far limited to the low hydrogen pressures (7, 23). We started therefore a systematic investigation of pseudobinary Laves alloys like $R(Mn_xFe_{1-x})_2$ under high hydrogen pressure in search of novel hydrides with possibly high hydrogen content. One of our goals is the determination of areas of existence of the orthorhombic RFe_2H_5 - based and cubic RMn_2H_6 – based hydrides in the $R(Mn_xFe_{1-x})_2$ – hydrogen system. The first step was treatment of ErMnFe alloy under high hydrogen pressure and characterization of received hydride by synchrotron XRD (X-ray diffraction), XANES (X-ray absorption near edge structure) and SQUID (Superconducting quantum interference device) to understand their crystal and electronic structures and magnetic properties.

實驗方法 (Experimental)

ErFeMn alloy was synthesized from pure metals (99.9%) by arc melting technique on a water cooled copper hearth to get the high purity single phase alloy. Synthesized solid solutions were annealed in tubular furnace at 800°C under vacuum for five days to get good homogeneity. Metallic alloys were crushed into fine pieces to record XRD. The powder X-ray diffraction was performed on a PW 1710 Philips diffractometer with Cu K alpha radiation.

Alloys were placed in a high pressure apparatus and heated at 100 °C in vacuum before hydrogen charging to remove any water molecules adsorbed on the surface of the alloys. Hydrogenation was performed under controlled conditions of temperature and pressure to get maximum amount of hydrogen into the alloys. After completion of the experiments hydrides were removed and stored in liquid nitrogen, to prevent any desorption immediately after the hydrogenation, for further investigations. Hydrogenated alloys were also characterized by XRD, XANES and SQUID.

結果與討論 (Results and Discussion)

The calculated and experimental room temperature XRD patterns of ErFeMn and $ErFeMnH_{4.7}$ are presented in figure 1(a) and 1(b), respectively. Since light hydrogen atoms have low X-ray scattering power, the pattern was refined assuming that only heavy Er, Fe and Mn atoms are involved in the diffraction intensity. The $ErFe_2$ crystallizes in C15 ($MgCu_2$) type cubic structure whereas $ErMn_2$ crystallizes in C14 ($MgZn_2$) hexagonal phase. In the present investigation ErFeMn XRD pattern was indexed in a cubic structure and the structure was refined on the basis of the Fd-*3*m space group by the Rietveld method (24). In figure 1 (b), the XRD pattern of $ErFeMnH_{4.7}$ shows a relative peak shift which corresponds to an increase of the unit cell parameter from 7.3771 (13) Å of ErFeMn to 8.1176 (22) Å of $ErFeMnH_{4.7}$ and relative volume expansion of about 30%. It means that in spite of high hydrogen pressure treatment, the lattice parameter and the concentration of hydrogen in the resulting hydride were only slightly

higher from those for samples hydrogenated at much lower pressure (a = 8.004 ′ and 4.6 H atoms p.f.u.). In C15 type structure three kinds of tetrahedral interstitial sites are available for hydrogen occupation: A_2B_2, AB_3, and B_4 (see inset in Figure 1a) in which A_2B_2 sites are more favourable for hydrogen bonding, so they should be filled first (25, 26). In this investigation experiment was conducted at 7 kbar and concentration of hydrogen reached 4.7 H atoms per formula unit. From the XRD patterns it seems that clear single phase peaks exist and there is no distortion in the crystal structure as in the case of RMn_2H_x and RFe_2H_x compounds (when $3.5 \leq x \leq 4.5$) in which rhombohedral or monoclinic distortion was observed (27). The absence of structural distortion is an indication that the absorption of hydrogen occurs mainly into all available A_2B_2 sites with little occupation in other AB_3 sites.

Figure 2(a) shows the Mn K-edge XANES spectra of ErFeMn and its hydride along with a Mn standard foil for comparison. Having reference spectrum as a finger print at the absorption edge, it is possible to use it as a standard for oxidation state and site symmetry. K-edge XANES spectra are due to the excitation process of 1s core electrons to the higher 4p manifold electronic states. Additionally the difference between energy values corresponding to normalized absorption μ_x near half-height usually indicates the change in oxidation state, but it should be considered that the comparison is applicable only when the atoms are present in the same or similar coordination environment (4). However, in the present case, this point is located far above the Fermi level and the difference could originate from the interference of multiple-scattering contributions at the neighbouring atoms. Therefore, its shift can be more associated with the variation of the structure or the lattice constant (as observed from XRD), than with a change of the ions charge. Similar behaviour was observed in the case of Fe K edge of ErFeMn and $ErFeMnH_{4.7}$ as shown in figure 3(a). Thus the charges on Mn/Fe in ErFeMn are mostly the same as in metal foil and remain nearly the same or increase slightly upon hydrogenation, as follows from the behaviour of the pre-edge peak. Figure 2(b) shows the second derivative function of Mn K edge for each ErFeMn alloy and $ErFeMnH_{4.7}$. The zero crossing of

main absorption features which represents the inflection point energy was found to be 6539.13 and 6539.40 eV for the alloy and hydride respectively. Figure 3(b) shows the second derivative function of Fe K edge for ErFeMn and $ErFeMnH_{4.7}$ and respective inflecton point energy was found to be 7112.34 and 7112.85 eV. The decrease in the intensity and change of the shape of spectra was observed for $ErFeMnH_{4.7}$ in both the cases. According dipolar selection rules, K-edge corresponds to an electronic transition from the 1s core state to the empty p states. Thus the XANES spectrum probes the empty projected local electronic density of p-state (10). The Mn 4p states of ErFeMn are hybridized with partially filled Mn 3d states near Fermi level which results in appearance of prominent peak at pre-edge region. Therefore due to hydrogenation, hydrogen acts as an electron donor and filled up these empty 3d states and reduced the peak intensity as the number of hydrogen increases per formula unit. This action decreases the number of 3d holes and pushes the 3d band below Fermi level resulting in drastic reduction of the pre-edge feature (28). Additionally, the large cell volume increase of the hydride compared to the intermetallic, can also reduce the 4p-3d hybridization and therefore the prepeak intensity (10).

The temperature dependent magnetic susceptibility (χ) and $1/\chi$ *vs.* temperature plots of ErFeMn are presented in figure 4(a) and (b), respectively. When the sample was cooled down from room temperature under magnetic field (1 kOe), the T_c (Curie temperature) was found to be at around 220 K from figure 4(b). Below T_c the material transforms into a strong ferromagnet at 5 K which is supported by hysteresis loops measurement (figure 5). Two more hysteresis curves are measured at 280 K and 100 K are shown in figure 5 in which alloy acts as paramagnetic and ferrimagnetic, respectively. It may be attributed that when the temperature is reduced from room temperature, Fe-Fe exchange coupling become stronger which results in strong ferromagnetic character of whole alloy. Even though Er and Mn have some amount of magnetic moment contribution to the net moment at room temperature, that is very less when compared to strong ferromagnetic nature of Fe. However, at low temperature, the Er moment is not negligible, since it should reach at least 8 μ_B, if no crystal field effect is observed. Added to that, the Mn moment

strongly depends on its critical Mn-Mn interatomic distance. Thus pronounced net Fe moment due to strong Fe-Fe exchange coupling imparts strong ferromagnetic character to this material. Moreover, the Er-Er and Er-Fe interactions are not negligible, $ErFe_2$ is a ferrimagnetic compound. Since half Fe is substituted by Mn atom, a random distribution of the coupling between the Fe and Mn moment should be observed. For zero field-cooled magnetization (ZFC) measurements, the sample was first cooled from room temperature to 5 K in a zero field. After applying the magnetic field of 1000 Oe at 5 K, the magnetization data were recorded in the warming cycle with the field on. For field-cooled magnetization (FC) measurements, the sample was cooled in an applied field of 1000 Oe (the same field as used for zero-field-cooled measurements) to 5 K and magnetization data were recorded in the warming cycle under the same field. The ZFC-FC magnetic susceptibility of $ErFeMnH_{4.7}$ at 1000 Oe, shown in figure 6(a) indicates a strong decrease of the magnetic susceptibility compared to the parent intermetallic and a weak hysteresis effect, which reveals a drastic change of magnetic structure upon H absorption. In addition the strong difference between ZFC and FC curves (figure 4) may be an indication of some spin glass behavior.

The reverse susceptibility of 15 kOe as shown in figure 6(b) can be fitted with a Curie constant of 15.8 emu/mole·Oe, an effective moment of 11.2 μ_B and a paramagnetic Curie temperature of 25 K. This means a paramagnetic behaviour with an effective moment larger than that expected for Er (9.5 μ_B). A contribution of Fe and Mn effective moments should also contribute to this constant. This fact is supported by the hysteresis measurements at two different temperatures, 280 K and 5 K, in which it is observed that the hydride appeared to be paramagnetic and weak antiferromagnetic, respectively (figure 7). Thus the hydrogenation of ErFeMn causes the huge reduction of magnetic susceptibility. Similar reduction in magnetic susceptibility has been observed on account of hydrogen insertion in YFe_2 hydride in our earlier studies (29). The investigation of magnetic properties for YFe_2 hydrides suggested the initial increase of magnetization moments for $x = \sim 3$ and the moment decreases further for higher

values of x. The volume effect is observed for x = ~ 3 with an increase in magnetization due to enhanced localization of the 3d orbitals of Fe. However for higher content of hydrogen the chemical role of hydrogen becomes dominant over volume expansion effect resulting in the decrease of magnetic moment values. In this case the loss of magnetic moment for higher content of the hydrogen was attributed to increased Fe-H bonding. The calculations using local spin density functional theory supports the larger bonding with hydrogen. As hydrogen content increases the bonding of Fe-H becomes more prevalent and becomes as large as ferromagnetic contribution from Fe-Fe and drops to minimum at Fermi level as against E_F observed in the case of parent alloy. The spin pairing of Fe with H with increasing hydrogen content upto x = 5 results in the loss of the magnetic moment. In the present case, the loss of magnetic moment of $ErFeMnH_{4.7}$ may be related either to the filling up of the Fe/Mn conduction band by the additional hydrogen electrons, decreasing the DOS near the Fermi level, or to the weakening of Fe-Fe interaction due to the considerable enlargement of the lattice parameters as observed from XRD. Another important factor is the coupling tendencies between the magnetic moments which are reported as Mn-Mn: antiferromagnetic, Mn-Fe: antiferromagnetic and Fe-Fe: ferromagnetic (30, 31). Based on this fact, the competing coupling tendencies results in rapid drop in T_c as well as overall magnetic moment. Cadavez-Peres *et al.* (32) have studied the competition between ferromagnetic and antiferromagnetic interactions in $Y(Mn_{1-x}Fe_x)_2D_{4.3}$ Laves hydrides and observed that for $0.1 < x < 0.85$ there was a loss of long range magnetic order. Only short range order due to ferromagnetic and antiferromagnetic interactions were observed with correlation length of 5 Å for x = 0.5. A similar behaviour is therefore expected in $ErMnFeH_{4.7}$.

結論 (Conclusions)

ErFeMn alloy and its hydride $ErFeMnH_{4.7}$ (synthesized under high hydrogen pressure) were characterized by XRD, XANES and SQUID. XRD patterns show that both alloy and hydride are in pure cubic phase. Rietveld refinement of XRD patterns shows considerable

increase in lattice parameter which results in about 30% cell volume expansion due to the absorption of hydrogen into the interstitial sites of crystal lattice. In spite of very high hydrogen pressure during the synthesis of hydride we did not receive novel structure, nor orthorhombic (like $ErFe_2H_5$) neither Fm3m cubic (like $ErMn_2H_6$). However the lattice expansion and hydrogen concentration were higher than reported so far for hydride formation in this intermetallic compound. Mn and Fe K-edge XANES study of alloy and its hydride indicates that the charge on Mn/Fe metal atoms present in the hydrides are mostly the same as in metal foil and remain nearly the same or increase slightly upon hydrogenation, as follows from the behaviour of the pre-edge peak. Magnetization measurement of $ErFeMnH_{4.7}$ by SQUID reveals that magnetic moment decreases to a larger extent by hydrogenation than by its parent compound. It is attributed to the weakening of Fe-Fe magnetic coupling and filling up of Fe/Mn conduction band by electrons from hydrogen atom.

計畫成果自評 (Evaluation of the project)

We have successfully fulfilled our goals in the last phase of the research plan in which the results have already been published in New Journal of Physics (33).

謝誌 (Acknowledgement)

The author would like to thank National Science Council (Grant Nos: NSC 95-2113-M-002-003; NSC 94-2811-M-002-007) for financial support.

參考文獻 (References)

1. Dantzer P 2002 *Mater. Sci. Eng.* **313** A329
2. Paul-Boncour V, Filipek S M, Percheron-Guegan A, Marchuk I and Pielaszek J 2001 *J Alloys Comp.* **317-318** 83.

3. Filipek S M, Paul-Boncour V, Percheron G A, Jacob I, Marchuk I, Dorogova M, Hirata T and Kaszkur T 2002 *J. Phys. Cond. Matter* **14** 11261**.**
4. Wang C Y, Paul-Boncour V, Kang C C, Liu R S, Filipek S M, Dorogova M, Marchuk I, Hirata T, Percheron G A, Sheu H S, Jang L Y, Chen J M and Yang H D 2004 *Solid State Commun.* **130** 815.
5. Paul-Boncour V, Filipek S M, Dorogova M, Bouree F, Andre G, Marchuk I, Percheron G A and Liu R S 2005 *J. Solid State Chem.* **178** 356.
6. Buschow K H J and van Diepen A M 1976 *Solid State Commun.* **19** 79.
7. Gualtieri D M and Wallace W E 1977 *J. Less-Common Met.* **55** 53.
8. Bushow K H J and Sherwood R C 1977 *J. Appl. Phys.* **48** 4643.
9. Goncharenko I N, Mirebeau I, Irodova A V and Suard E 1999 *Phys. Rev.* B **59** 9324.
10. Paul-Boncour V and Percheron-Guegan A 1999 *J. Alloys Comp.* **293-295** 237.
11. Yamada H and Shimizu M 1986 *Phys. Lett.* A **117** 313.
12. Fuji H, Saga M and Okomoto T 1987 *J. Less-Common Met.* **130** 25.
13. Figiel H, Przewoznik J, Paul-Boncour V, Lindbaum A, Gratz E, Latroche M, Escorne M, Percheron-Guegan A and Mietniowski P 1998 *J. Alloys Comp.* **274** 29.
14. Figiel H, Budziak A, Zakariasz P, Zukrowski J, Fischer G and Dormann E 2004 *J. Alloys Comp.* **368** 260.
15. Makarova O L, Goncharenko I N, Irodova A V, Mirebeau I and Suard E 2002 *Phys. Rev.* B **66** 104423
16. Fruchart D, Berthier Y, De Saxce T and Vuillet P 1987 *J. Less-Common Met.* **130** 89.
17. Deryagin A V, Kudrevatykh N V, Moskalev V N and Mushnikov N V 1984 Fiz. Met. Metalloved. **58** 1148.
18. Rhyne J J, Fish G E, Sankar S G and Wallace W E 1979 *J. Physique* **40** 209.
19. Paul-Boncour V, Giorgetti C, Wiesinger G and Percheron-Guégan A. 2003 *J. Alloys Compds.* **356-357** 195

20. Kierstead H A 1980 *J. Less-Common Metals* **71** 303.

21. Shashikala K, Raj P and Sathyamoorthi A 1996 *Mater. Res. Bullet.* **31** 957.

22. Paul-Boncour V, Filipek S M, Marchuk I, André G, Bourée F, Wiesinger G and Percheron-Guégan A 2003 *J. Phys.: Cond. Matter.* **15** 4349.

23. Sankar S G, Gualtieri D M and Wallace W E 1978 *The Rare Earth in Modern Science and Technology* (G.J. Mc Carthy and J.J. Rhyne Edts), Plenum, New York, , 69.

24. Larson A C and von Dreele R B 1994 *Generalized Structure Analysis System (GSAS)*; Los Alamos National Laborator Report LAUR, 1994.

25. Fruchart D, Rouault A, Shoemaker C B and Shoemaker D P 1980 *J. Less-Common Met.* **73** 363.

26. Irodova A V, Lavrova O A, Laskova G V and Padurets L N 1982 *Sov. Phys. Solid State* **24** 41.

27. V. Paul-Boncour 2004 *J. Alloys Comp.* **367** 185.

28. Cibin G, Marcelli A, Battisti M, Chaboy J, Piquer C and Bozukov L 1999 *J. Mag. Mag. Mater.* **196-197** 671.

29. Paul-Boncour V and Matar S F 2004 *Phys. Rev.* B **70** 188435.

30. Kouvel J S 1965 *J. Appl. Phys.* **36** 980.

31. Bechman C A, Narashimhan K S V L. Wallace W E, Craig R S and Butera R A 1976 *J. Phys. Chem. Solids* **37** 245.

32. Cadavez-Peres P, Goncharenko I and Mirebeau I 2002 *Appl. Phys.* A **74** S692.

33. Mylswamy S, Drozd V, Liu R S, Bagkar N C, Chou C C, Sun C P, Yang H D, Paul-Boncour V, Marchuk I, Filipek S M, Sheu H S and Jang L Y 2007 *New J. of Phys.* **9** 271.

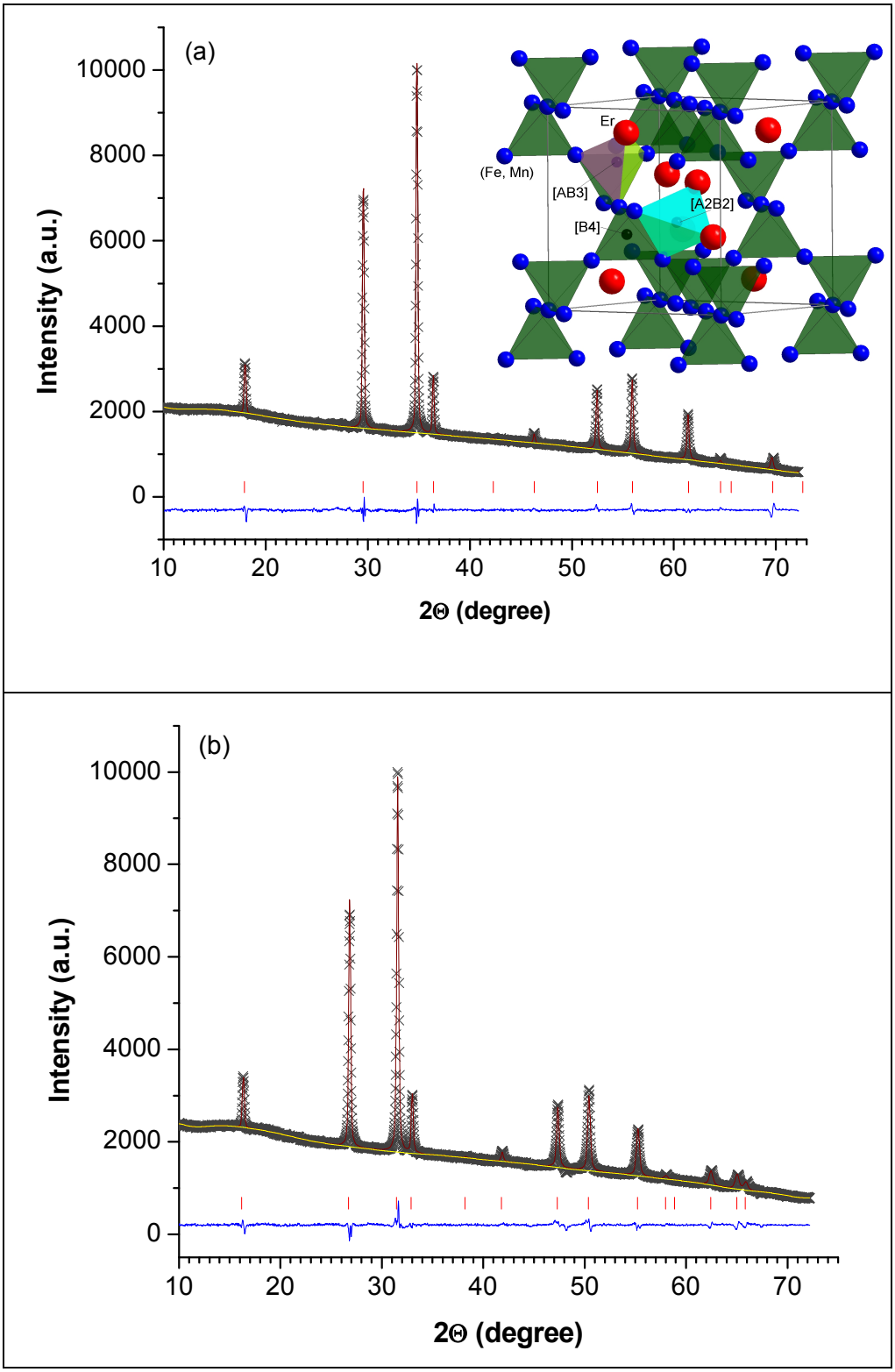

Figure 1 Calculated (+) and experimental (-) XRD patterns of (a) ErFeMn and (b) $ErFeMnH_{4.7}$. Inset shows C15 crystal structure of ErFeMn.

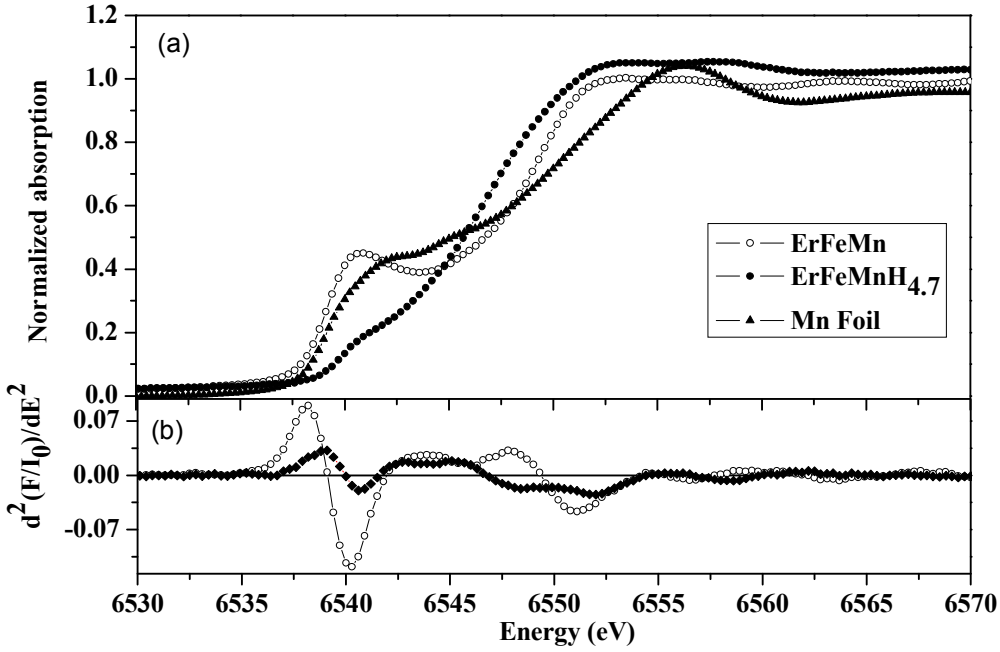

Figure 2 (a) Mn K-Edge XANES plots of ErFeMn and $ErFeMnH_{4.7}$ compared with standard Mn foil and (b) second derivative function for ErFeMn and $ErFeMnH_{4.7}$

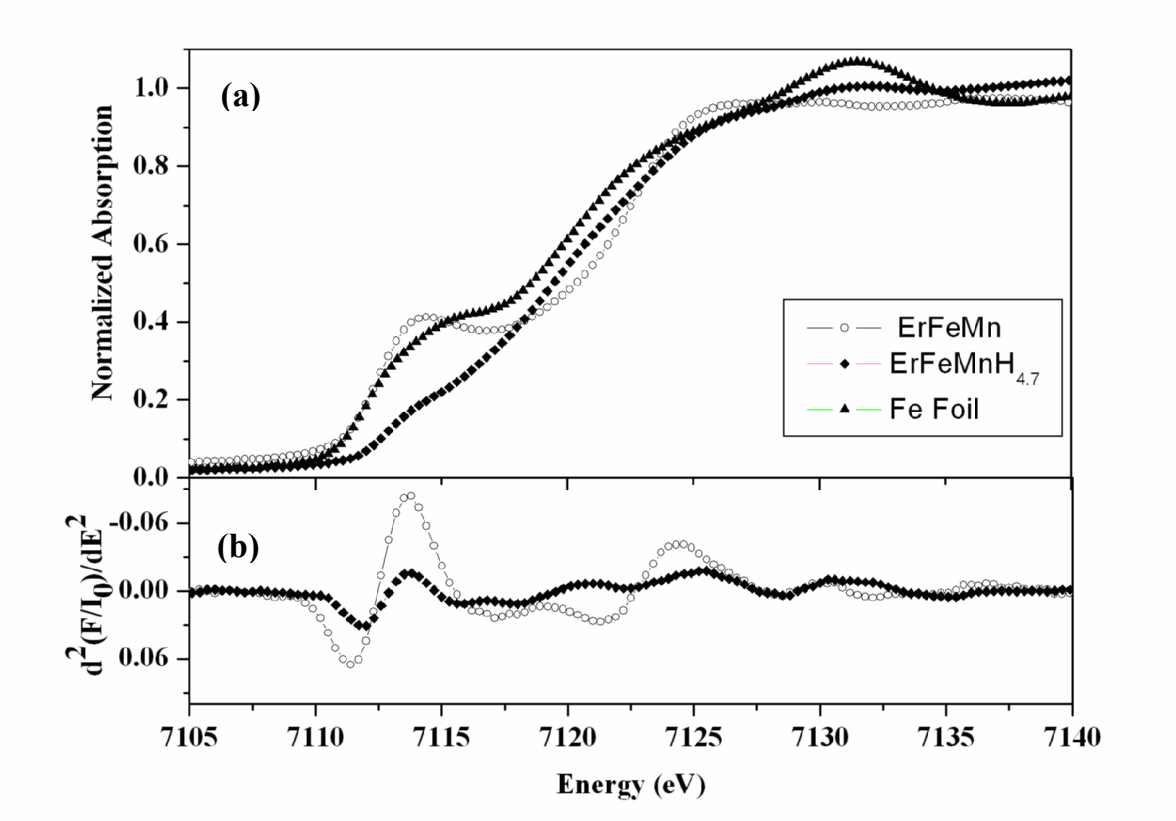

Figure 3 (a) Fe K-Edge XANES plots of ErFeMn and $ErFeMnH_{4.7}$ compared with standard Fe foil and (b) second derivative function for ErFeMn and $ErFeMnH_{4.7}$

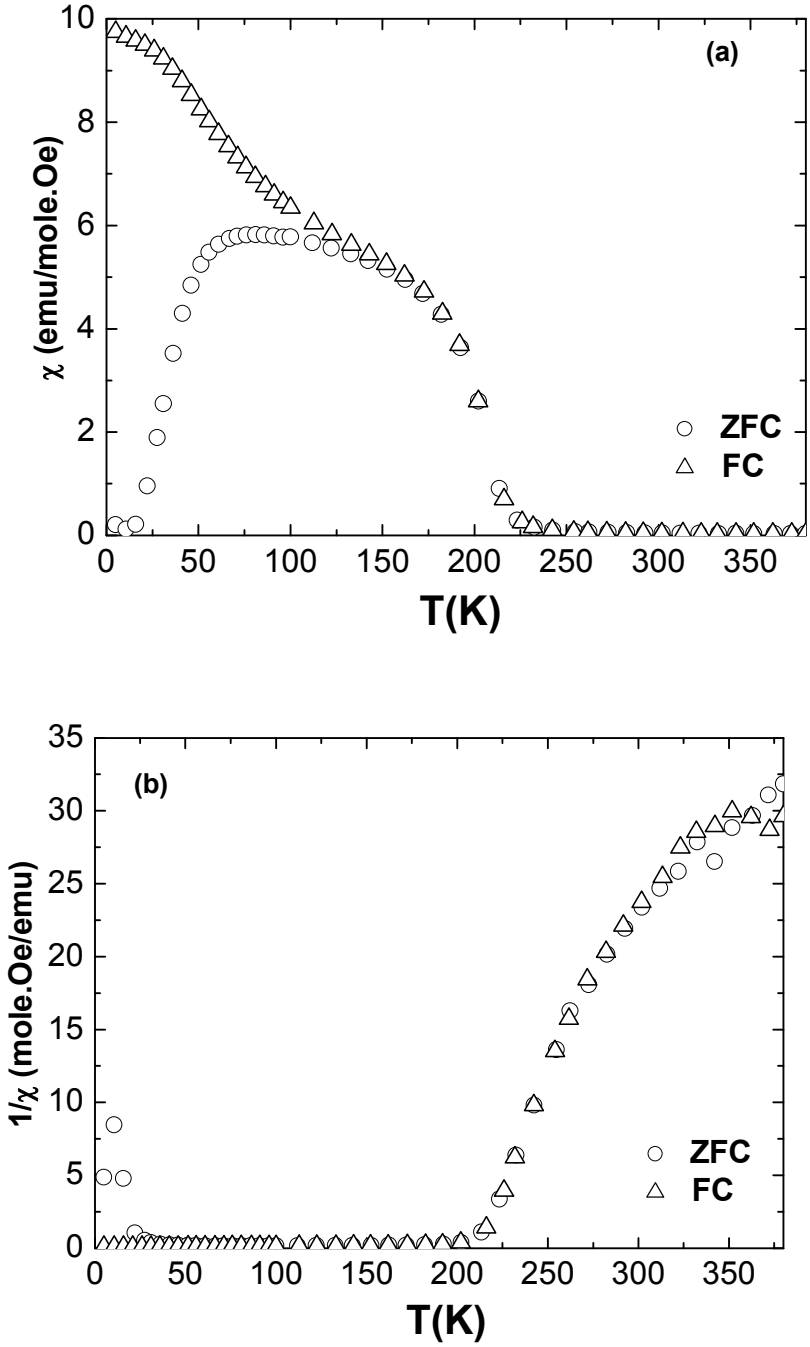

Figure 4 (a) Temperature dependent magnetic susceptibility (χ) of ErFeMn and (b) 1/χ *vs.* temperature plot of ErFeMn measured at 380 K in 1000Oe external magnetic field.

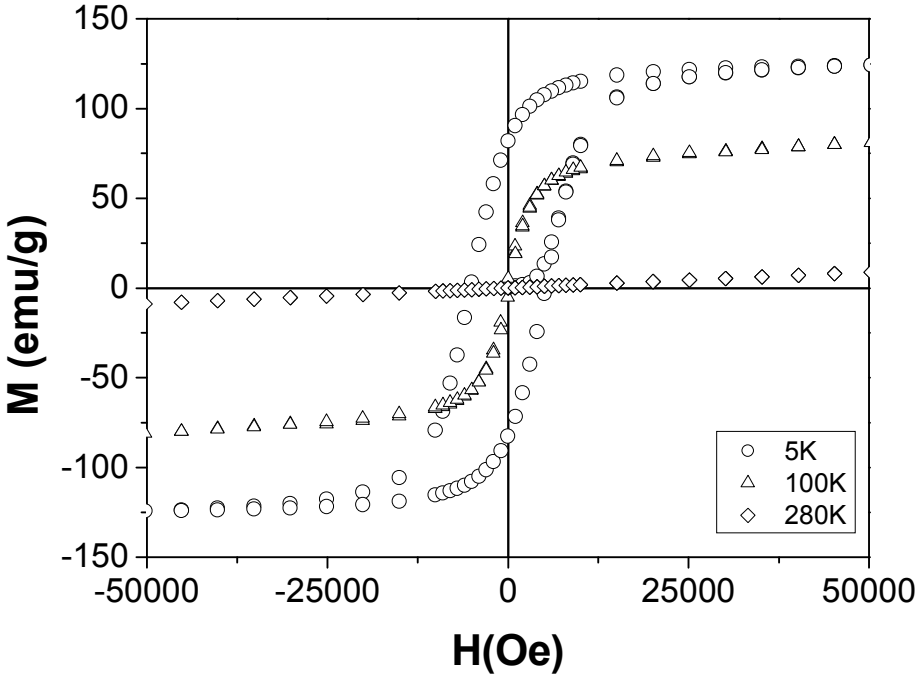

Figure 5 Hysteresis loops of ErFeMn at 5 K, 100 K and 280 K.

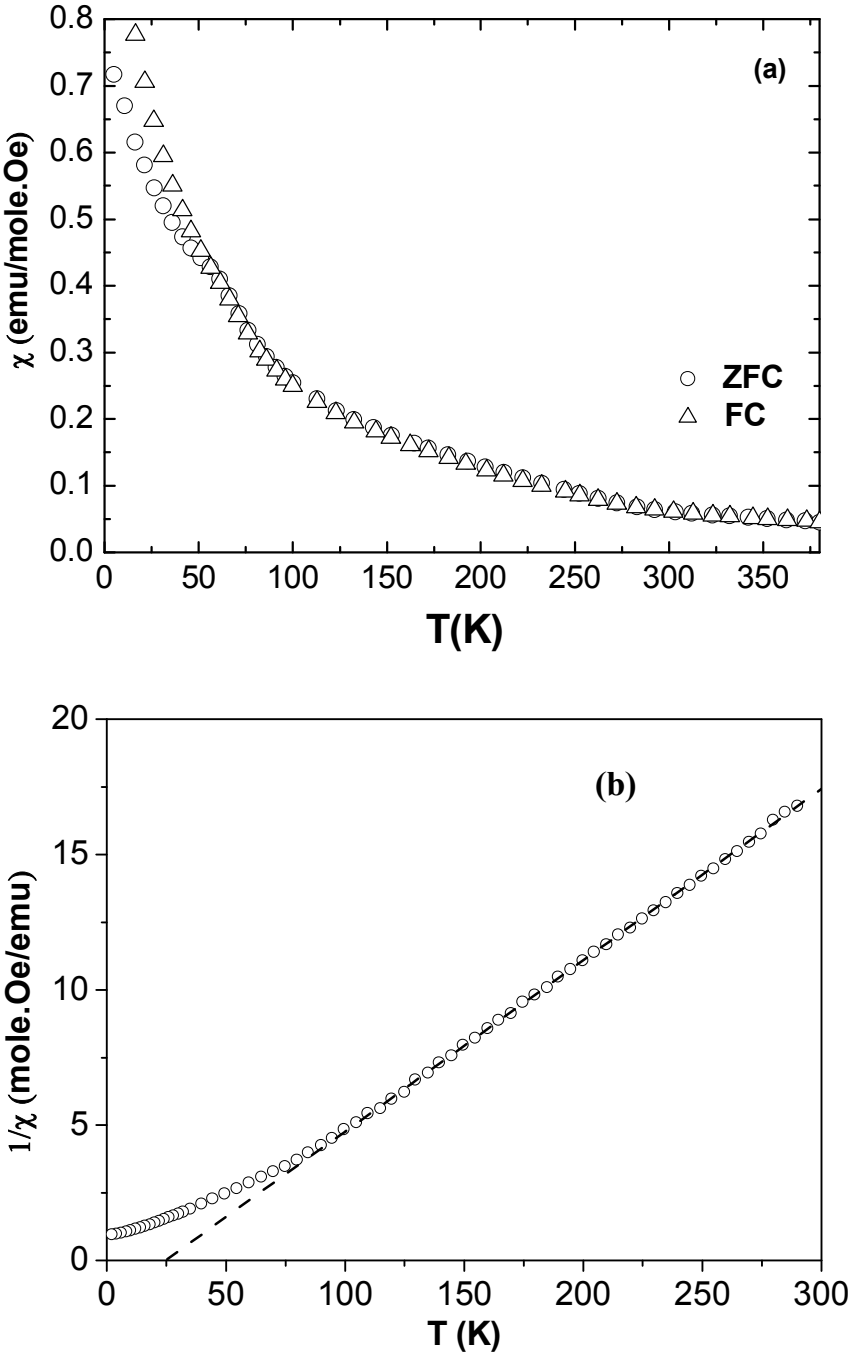

Figure 6 (a) Temperature dependent magnetic susceptibility (χ) of $ErFeMnH_{4.7}$ and (b) 1/χ *vs.* temperature plot of $ErFeMnH_{4.7}$ measured at 15 kOe (o) fitted with a Curie Weiss law (---).

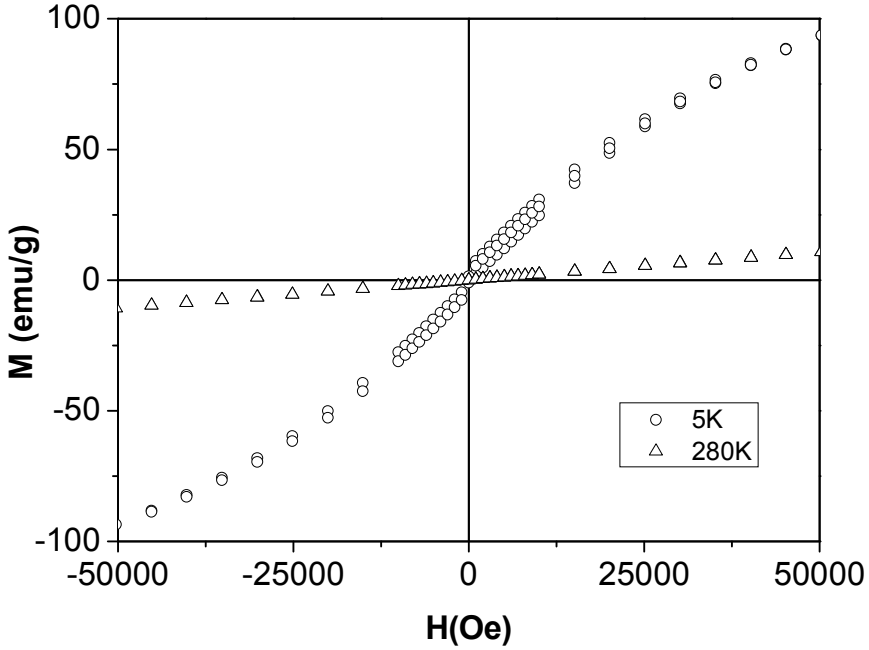

Figure 7 Hysteresis loops of $ErFeMnH_{4.7}$ at 5 K and 280 K

行政院國家科學委員會補助專題研究計畫

利用高壓合成新穎氫化物材料及其特性分析

[台波國合計畫(2/2)]

出國研究心得報告

計畫編號：NSC 95-2113-M-002-003
出國期間：95 年 8 月 26 日至 95 年 9 月 18 日

出國人員：

劉如熹　台灣大學化學系（計畫主持人）

Nitin Bagkar　台灣大學化學系（博士後研究員）

中 華 民 國 九 十 五年 十 月

POLAND VISIT REPORT

I. Visit to Institute of Physical Chemistry, Polish Academy of Sciences:

Name : Nitin Bagkar

Period : 08/26/2006 to 09/18/2006

Arrived at Poland on 26th August and joined in Institute of Physical Chemistry, Polish Academy of Science, Warsaw, Poland on 28th August for training in high pressure synthesis with Prof. S. M. Filipek.

A. Learning the operation of high pressure apparatus:

The basic operation of high pressure equipment was demonstrated by Prof. Filipek including the cleaning procedures and safety measures in detail during the first week of training. The typical setup used for high pressure is shown in figure 1 (a) and 1 (b). The various parts of equipment contain hydrogen source (commercially available hydrogen cylinder), multiplicator and high pressure reactor. Hydrogen cylinder was connected to multiplicator where the hydrogen gas was compressed to very high pressures through heavy copper capillary tube which can withstand very high pressures of the order of 15 GPa. All joints of the capillary were connected with metallic ferrules and rubber sealing to avoid pressure leakages during reaction. The output of the multipilcator was connected to the reactor multiplicator through the capillary. The reactor multiplicator was connected to vacuum line, reactor and the pressure gauge. The reactor is made up of heavy steel tube into which samples were loaded in small steel samples containers. One side of the steel tube is closed with threaded stopper and the other end is connected to multiplcator. Hydrogen inlet capillary is connected through small threaded hole near multiplicator. Steel tube is surrounded by external electric heating coil to get desired reaction temperature. The assembly of the high pressure was protected with the toughened glass windows as a safety measure.

B. Experiments carried out during Poland visit

It was planned to prepare manganese hydride and their Laves phase hydride with ErHx under high pressure. The samples of manganese powder and Erbium lumps were loaded into small steel containers and placed into the heavy steel reactor tube. One side of the tube was connected to the vacuum pump through multiplicator. Hydrogen inlet copper tube is connected through a small threaded hole near multiplicator. The samples were then evacuated with vacuum pump for three hours and hydrogen pressure was slowly increased from atmospheric pressure to 7000 atm.

The temperature is slowly increased to 125°C. Samples were left inside the reaction vessel for about 20 hrs. Then the temperature was reduced to room temperature by cooling the steel tube with liquid hydrogen and after complete cooling of the system the hydrogen pressure was slowly reduced to the atmospheric pressure. The samples were taken out of the vessel and used for further characterization using X-ray diffraction.

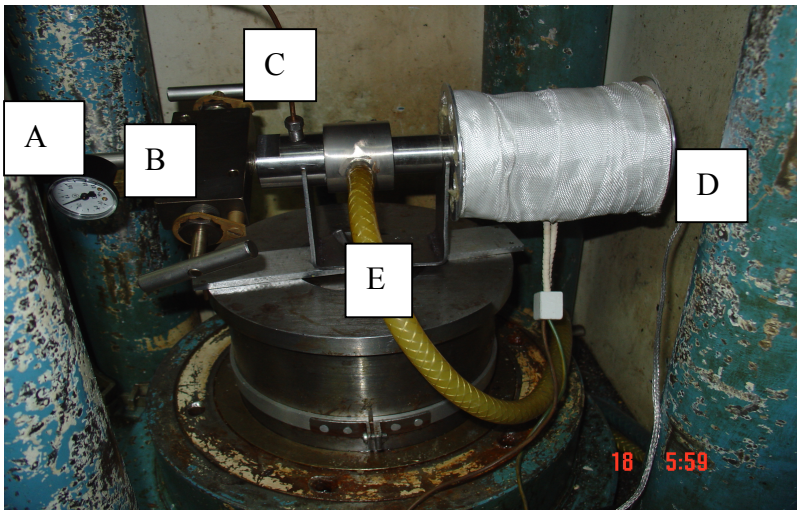

A. Pressure gauge B. Multiplicator C. Capillary D. External heater E. Cooling water circulation

Figure 1a. Experimental setup for high pressure synthesis

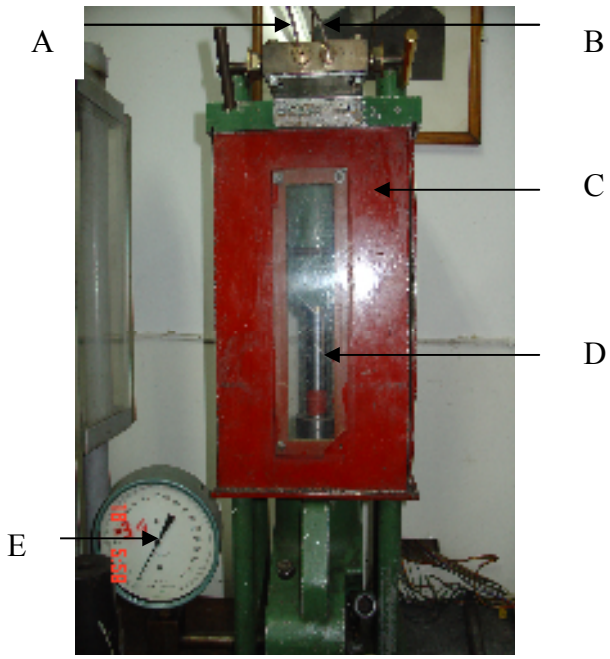

A. Copper capillary to reactor B. Copper capillary from hydrogen cylinder C. protecting shield D. Piston E. Pressure Gauge

Figure 1b. Multiplicator assembly to increase hydrogen pressure

C. Results and Discussions

X ray diffraction pattern for erbium hydride samples was shown in figure 1. The sample contains he oxide impurities as evident from the diffraction pattern. It also showed the formation of ErH_3 hydride having cubic phase. However for the manganese hydride the peak positions were not shifted as compared to peak positions of pure Mn powder. Powder XRD pattern of pure Mn powder and hydrogenated samples of Mn powder was shown in the figure 2. Thus there was very low amount of manganese hydride formation under present experimental conditions. This was due to low temperature used during hydrogenation indicating that higher temperature is required for the hydride formation in the case of MnH_x with higher hydrogen content.

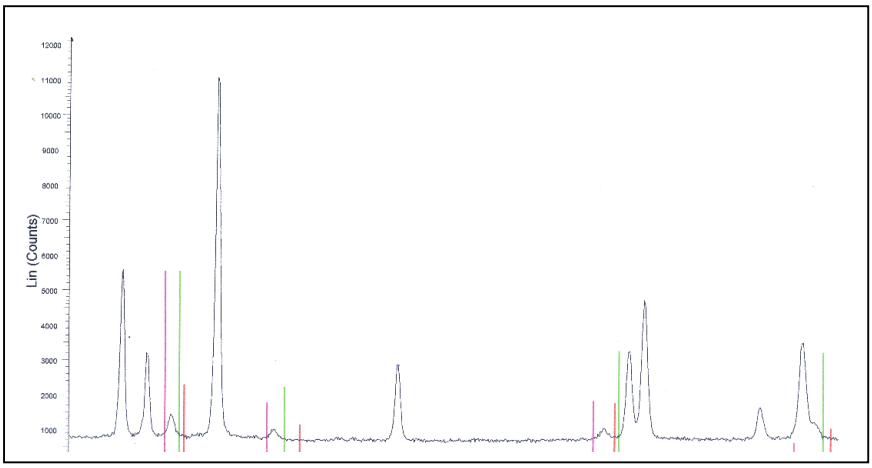

Figure 1. XRD pattern of ErH_x

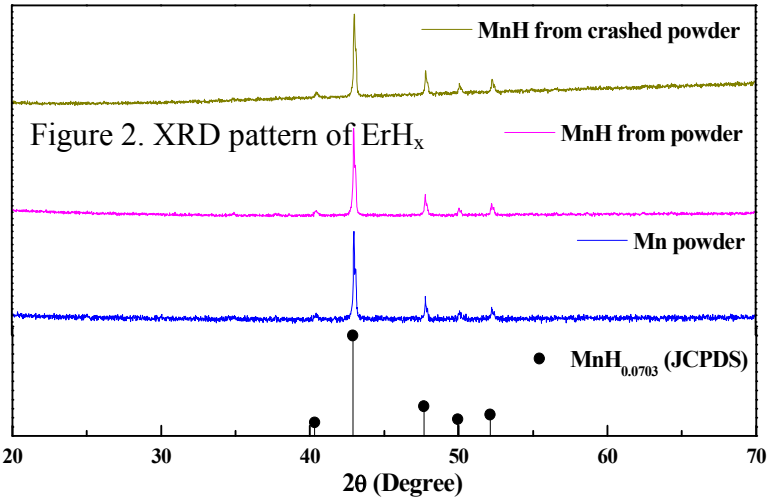

Figure 2. XRD pattern of MnH_x

II. Conference report:

Prof. Ru-Shi Liu attended International symposium on “E-MRS Fall Meeting 2006” from 3rd to 7th September in Warsaw, Poland. The conference was organized in Warsaw Institute Technology, Poland and he presented the poster on "The Study of Growth Mechanism of Gold Nanorods".

(i) Overview of the symposium:

Symposium was organized into ten sections like nanostructured composite films, nanomaterials in catalysis, doped nanomaterials and it also included Fall school on thermal analysis, Thin layered materials workshop, exhibitors and technology commercialization market place. About 850 delegates from all over the world were participated in the E-MRS meet of which 14 delegates were from Taiwan. There were 29 planery sessions and approximately 10 invited talks in each section. During the conference Prof. Ru-Shi Liu attended important lectures and oral presentations related to our area of research through out the symposium. He had good interaction with participants and developed some good ideas based on the new developments for our future work. The Fall meeting was particularly useful in developing good understanding of the structural features, magnetic properties and thermal properties of technologically advanced materials.

(ii) Our contribution in the conference:

Prof. Ru-Shi Liu has presented a poster on “The Study of Growth Mechanism of Gold nanorods". In his poster he presented a novel approach to fabricate long length of gold nanorods by controlling the volume of growth solution. The essence of poster lies in the demonstration of growth mechanism of gold nanorods by X-ray absorption spectroscopy. Because of which his poster attracted good number of participants and bagged the award of the best poster for the symposium. The abstract of the poster was given at the end.

III. Comments:

(i) Visit to the Institute of Physical Chemistry by Dr. Nitin Bagkar:

I was impressed by the hospitality of Prof. Filipek with a warm welcome at Warsaw airport followed by a good guidance and instruction throughout my stay in Institute of Physical Chemistry, Polish Academy of Sciences. I was fortunate to interact with his group members, who helped me a lot during my stay at the institutes in all aspects. I learnt a lot from Prof. Filipek, especially the synthesis of novel hydride materials by high pressure technique and controlling the reaction conditions (temperature and pressure) which is very crucial for the synthesis of metal hydrides.

(ii) Discussions with Prof. R. S. Liu and Prof Filipek:

The Poland visit by Prof. Ru-Shi Liu and Dr. Nitin Bagakar was very productive from the point of view of the discussion regarding the continuation of project with Prof. Filipek. During the discussions we acquired a very good knowledge in the advance developments of high pressure synthesis and novel metal hydrogen systems. Moreover, we discussed the status of our project with Prof. Filipek during our visit. Prof. Ru-Shi Liu also planned the new proposal for submitting to the National Science Council and finalized the project with Prof. Filipek. Altogether visit to Poland was very fruitful in terms of the implementation of good synthetic methods based on the training in Poland and interactions in the conference for the future work in Taiwan.

IV. Materials brought back from Poland:

The proceeding of the Symposium on "E-MRS Fall Meeting 2006"

Group photo: Dr. Bagkar, Prof. Filipek and Prof. Liu outside the Institute of Physical Sciences, Warsaw, Poland. (12/09/2006)

Poster at E-MRS Fall Meeting 2006, Symposium B,

The Study of Growth Mechanism of Gold Nanorods

Ru-Shi Liu [1], Hao Ming Chen[1], Shu-Fen Hu [2], Stansiław Filipek [3]

1. National Taiwan University, Department of Chemistry, Sec. 4, Roosevelt Road, Taipei 10617, Taiwan
2. National Nano Device Laboratories (NDL), No. 26, Prosperity Road I, Science-based Industrial Park, Hsinchu 30078, Taiwan
3. Institute of Physical Chemistry, Polish Academy of Sciences, Institute of Physical Chemistry, Kasprzaka 44/52, Warszawa 01-224, Poland

Abstract:

A new approach to fabricate long length of gold nanorods by controlling the volume of growth solution will be reported. The shape evolutions ranging from fusiform nanoparticles to 1-D rods were observed. Increasing the addition of growth solution can control the length of nanorods. The length of rods can be extended to 2 μm, and nanorods with aspect ratios of up to ~ 70 could be obtained. Moreover, X-ray absorption spectroscopy (XAS) is applied herein to elucidate the growth mechanism of gold nanorods. The gold ions were directly reduced to gold atoms by ascorbic acid during the reaction, and then gold atoms were deposited on the surface of gold seeds that were introduced into the reaction. Extended X-ray absorption fine structure (EXAFS) confirmed the growth of gold and the environment around Au atoms over the reaction. The XAS are expected to have wide applications in the growth of gold and other related materials.